The potential of small unmanned aircraft systems and structure-from-motion for topographic surveys: A test of emerging integrated approaches at Cwm Idwal, North Wales

T.N.Tonkin[a1], N.G.Midgley[a] , D.J.Graham[b], J.C.Labadz[a]

[a]School of Animal, Rural and Environmental Sciences, Nottingham Trent University, Brackenhurst Campus, Southwell, Nottinghamshire NG25 0QF, UK

[b]Polar and Alpine Research Centre, Department of Geography, Loughborough University, Leicestershire LE11 3TU, UK

[1]Corresponding author. Tel.: + 44 115 848 5257. toby.tonkin@ntu.ac.uk

Abstract

Novel topographic survey methods that integrate both structure-from-motion (SfM) photogrammetry and small unmanned aircraft systems (sUAS) are a rapidly evolving investigative technique. Due to the diverse range of survey configurations available and the infancy of these new methods, further research is required. Here, the accuracy, precision and potential applications of this approach are investigated. A total of 543 images of the Cwm Idwal moraine-mound complex were captured from a light (< 5 kg) semi-autonomous multi-rotor unmanned aircraft system using a consumer-grade 18 MP compact digital camera. The images were used to produce a

23   DSM (digital surface model) of the moraines. The DSM is in good agreement with

24   7761 total station survey points providing a total vertical RMSE value of 0.517 m and

25   vertical RMSE values as low as 0.200 m for less densely vegetated areas of the

26   DSM. High-precision topographic data can be acquired rapidly using this technique

27   with the resulting DSMs and orthorectified aerial imagery at sub-decimetre

28   resolutions. Positional errors on the total station dataset, vegetation and steep terrain

29   are identified as the causes of vertical disagreement. Whilst this aerial survey

30   approach is advocated for use in a range of geomorphological settings, care must be

31   taken to ensure that adequate ground control is applied to give a high degree of

32   accuracy.

33

34   **Highlights**

35   ▪   An integrated sUAS and SfM approach is used to generate high-resolution

36   topographic data.

37   ▪   SfM data compared with a total station ground survey.

38   ▪   Positional errors on the total station dataset, vegetation and steep terrain are

39   identified as causes of vertical difference between the two datasets.

40   ▪   The integration of a combined sUAS and SfM approach is discussed.

41

42   **Keywords**

43   Small unmanned aircraft system, Structure from motion, Digital surface model,

44   Digital elevation model, Topographic surveying

1 Introduction

The use of small unmanned aircraft systems (sUAS) and structure-from-motion (SfM) digital photogrammetry presents a new methodological frontier for topographic data acquisition and is of interest to scientists researching in a range of geomorphological environments (Westoby et al., 2012; Carrivick et al., 2013; Hugenholtz et al., 2013; Tarolli, 2014). Traditionally low-level aerial photography has been acquired using a variety of unmanned platforms including small lighter-than-air blimps, kites, and model fixed-wing and single rotor aircraft (e.g. Wester-Ebbinghaus, 1980; Rango et al., 2009; Smith et al., 2009; Hugenholtz et al., 2013). More recently lightweight (< 5 kg), relatively low-cost multi-rotor aerial platforms have been used to capture low-level imagery (Harwin and Lucieer, 2012; Niethammer et al., 2012; Rosnell and Honkavaara, 2012; Mancini et al., 2013; Lucieer et al., 2014). These sUAS can be programmed to fly semi-autonomously at fixed altitudes along flight lines, ensuring optimal image overlap for digital photogrammetry. A key strength of the integrated sUAS–SfM approach is the degree of automation involved. Previously, a high degree of user experience was a prerequisite for both the operation of aerial platforms and the application of photogrammetric methods to extract meaningful topographic data from aerial imagery (Aber et al., 2010). The premise of SfM as a digital photogrammetric technique is that three-dimensional coordinates can be extracted from sufficiently overlapping photography without the need for camera spatial information (Snavely et al., 2008; Westoby et al., 2012). The integration of SfM with sUAS camera platforms offers a rapid and increasingly cost effective option for geomorphologists to produce digital surface models (DSMs), with resolution and data quality proposed to be on-par with, or better than LiDAR (Carrivick et al., 2013; Fonstad et al., 2013). SfM based topographic surveys have

recently been used for a variety of geoscientific applications including quantifying rates of landslide displacement (Lucieer et al., 2013), mapping vegetation spectral dynamics (Dandois and Ellis, 2013), producing DEMs (digital elevation models) of agricultural watersheds (Ouédraogo et al., 2014), quantifying coastal erosion rates (James and Robson, 2012), and measuring rates of glacier motion and thinning (Whitehead et al., 2013). The potential of SfM to aid geomorphological mapping, derive measurements of landforms (morphometry) and quantify geomorphological change is evident. Numerous software packages for SfM are now available and include cloud-based processing, which has the additional benefit of not requiring a high-specification consumer computer capable of handling the image processing.

Whilst a range of recent studies have sought to quantify data quality and associated error of SfM techniques (Harwin and Lucieer, 2012; Turner et al., 2012; Westoby et al., 2012; Dandois and Ellis, 2013; Fonstad et al., 2013; Hugenholtz et al., 2013; Ouédraogo et al., 2014), further research is beneficial due to the diverse nature of the aerial platforms and consumer-grade digital cameras available for the production of topographic data using this methodology. Existing reports on the effectiveness of integrated multi-rotor based sUAS–SfM approaches describe surveys conducted from relatively low altitudes (< 50 m). The aims of this research are to: (1) provide a systematic account of the data acquisition process associated with this new integrated technique; (2) compare vertical spot heights obtained from the sUAS–SfM survey to those obtained from a total station ground survey; (3) highlight important considerations for researchers seeking to use sUAS and SfM approaches to acquire data for topographic investigations; and (4) provide a baseline for the potential

94 spatial resolutions when using a consumer-grade 18 MP compact digital camera at a

95 target flight altitude of 100 m.

96

97 **2 Study area**

98 The test was undertaken at Cwm Idwal, north Wales (53° 6′50.89″N; 4° 1′38.38″W;

99 Fig. 1) (Appendix A), a large cirque that was last occupied by a glacier during the

100 Younger Dryas Stadial (c.12.9-11.7 ka BP; Bendle and Glasser, 2012). The study

101 area is located on the cirque floor and covers an altitudinal range of ~ 370 to ~ 410

102 m (above ordnance datum). The geomorphology of the site is characterised by a

103 moraine-mound complex ('hummocky moraine') located on both the east and west of

104 Llyn [lake] Idwal (Fig. 1c). These moraines have been the subject of numerous

105 investigations (e.g. Darwin, 1842; Escritt, 1971; Gray, 1982; Addison, 1988; Graham

106 and Midgley, 2000; Bendle and Glasser, 2012) due to their importance for

107 understanding the significance of Younger Dryas glaciers in the British Uplands. The

108 majority of the moraines are 8 to 80 m in length, with the exception being a set of

109 discontinuous stream-breached ridges totalling ~450 m in length which are stacked

110 against the western cirque wall. In places the morphology of the moraines are

111 influenced by glacially abraded bedrock. The prominence of some landforms is also

112 disguised by a peat infill. The southern section of the survey area is characterised by

113 a relatively flat lake infill and steep glacially abraded bedrock slopes. Vegetation on

114 the eastern side of the Cwm is typically restricted to short swards of grass, whereas

115 livestock grazing exclosures erected in the 1950s and 1960s on the western side of

116 Llyn Idwal have promoted the growth of vegetation including a thick cover of

117 common heather (Calluna vulgaris), western gorse (Ulex gallii), and the occasional

118 rowan (Sorbus aucuparia) and silver birch (Betula pendala) (Rhind and Jones,

119 2003). A large part of the moraine-mound complex and surrounding area were

120 surveyed with a total station by Graham and Midgley (2000). A similar area was

121 surveyed by a sUAS to allow a direct comparison between total station based data

122 acquisition, and the sUAS–SfM method used for this study.

123

3 Methods and materials

3.1 Image Image and data acquisition

126 Aerial imagery was acquired using a Canon EOS-M 18 MP camera suspended from

127 a DJI S800 Hexacopter (Fig. 2). A Photohigher AV130 servo driven gimbal

128 maintained the camera angle close to the nadir. The hexacopter was equipped with

129 a Wookong-M GPS assisted flight controller which allowed for semi-autonomous

130 surveys. Survey flight-lines were pre-programmed via the DJI Ground-Station

131 software package. For all surveys the sUAS was set to a target altitude of 100 m

132 above ground level (AGL) and horizontal ground speed of 2.5 ms^{-1}. The target

133 altitude is calculated in the DJI Ground-Station software using elevation data derived

134 from Google Earth. Parallel flights lines were programmed to have an image sidelap

135 of 80%, whilst taking into account the camera sensor size (22.3 × 14.9 mm) and

136 focal length (22 mm). The intervalometer function of the Magic Lantern third-party

137 camera firmware was set to acquire imagery every 2 s along parallel flight lines.

138 Actual image acquisition was every ~ 4 s, resulting in image capture approximately

139 every 10 m along flight lines. Although image capture can be triggered using the DJI

140 flight controller, an intervalometer was used for its improved reliability and potential

141 to capture excess imagery along flight lines. This allowed for blurred or poor quality

142 imagery to be removed whilst ensuring that an image onlap in excess of 80% was

143 maintained. The camera was set to shutter-priority mode and used a 1/1000 s

144 shutter speed. To provide the required image coverage the survey area had to be

145 split between four flights. The sUAS had a flight-time of ~ 14 min whilst carrying its

146 payload (using an 11 Ah, 22.2 V, 6 cell lithium polymer battery). A generous

147 overhead (~ 2 min) was left in order to safely land the sUAS. In the UK unaided

148 visual line of sight (VLOS) has to be maintained whilst operating sUAS (CAA, 2012).

149 Therefore the ground equipment and launch position were moved between flights to

150 allow the sUAS to be easily observed, and manually controlled if necessary.

151

152 The total station dataset was acquired over multiple survey sessions in 1997 and

153 1998 using a Leica TC600 (Graham and Midgley, 2000). An assessment of error for

154 this data set is unavailable. However, measurement accuracies (expressed as

155 standard deviation) for the TC600 are defined by Leica (1997), with distance

156 measurements accurate to 2 mm ± 2 ppm and angle (horizontal and vertical)

157 measurements to 1.5 mgon. As the original total station dataset was collected for

158 the purpose of characterising the overall shape of the moraine-mound complex,

159 individual points were collected rapidly. Points recorded whilst the prism pole was

160 not perfectly vertical have the potential to result in misregistration between the two

161 datasets. The extent of the resulting error will be exacerbated by slope steepness

162 and the height of the reflector on the detail pole. The SfM dataset was tied into the

163 same arbitrary co-ordinate system and datum through the use of two brass pin

164 benchmarks located on exposed bedrock on the east and west of Llyn Idwal. Point

165 densities for the validation points reach as high as 20 per 100 m2 over the moraine-

166 mound complex (Graham and Midgley, 2000). For the sUAS survey, 19 SfM ground-

167 control points (GCPs) were distributed across the survey area (Fig. 3a). White

168 laminated A3 size targets (297 × 420 cm) were used as GCPs and were found to be

169 adequately visible on the aerial imagery. These GCPs were surveyed with a Leica

170 TC407 total station to a precision of ≤ 1 mm and estimated accuracy of < 3 cm.

171

172 *3.2 Image processing and analysis*

173 From the original set of 824 images, 543 images were selected for model

174 reconstruction using the Agisoft Photoscan 1.0.0 (build 1795) software package.

175 Images were visually assessed for quality and blurry images were removed prior to

176 processing. Image processing followed the recommended procedure outlined by

177 Agisoft (2013). Image processing was conducted on a HP Z820 workstation

178 equipped with dual Intel Xeon E5-2690 processors, 128 GB RAM, and nVidia 680

179 graphics card. As GPS information for camera positions were not collected, images

180 were aligned using the 'Generic Pair Preselection' parameter. This parameter

181 detects matching features between images at a lower accuracy first, to reduce

182 overall processing time (Agisoft, 2013). Photoscan provides nominal parameters for

183 setting the target accuracy to which the images are aligned. Here the 'high' setting

184 was used to obtain the best possible image alignment accuracy. Nineteen GCPs

185 were then identified on imagery within the software a total of 674 times, with the XYZ

186 coordinates input for each point. The sparse point cloud was optimised using a

187 marker accuracy of 0.001 m and focal parameters (F_y and F_x) defined in the image

188 headers. Camera radial and tangential distortion coefficients (K_1, K_2, K_3, P_1 and P_2)

189 were automatically estimated by Photoscan. A dense point cloud was then produced

190 using the 'medium' quality setting. Again, this is a nominal setting that relates to the

191 geometric accuracy of the target dense point cloud produced within Photoscan.

192 Aggressive depth filtering was used to remove outliers from the dense point cloud

193 (Agisoft, 2013). The dense point cloud and polygonal mesh was generated using a

194 target point count of 3×10^5. An additional sparse point cloud and a DSM were

195 produced for comparative purposes. An orthorectified aerial image was produced

196 using the 'orthophoto' and 'mosaic' parameters with colour correction enabled.

197 Where image overlap occurs, the 'mosaic' parameter ensures that images with pixels

198 closest to the image centre are used preferentially for orthophoto generation (Agisoft,

199 2013).

200

201 Data handling and the analysis of geographic data were conducted using

202 QuantumGIS 2.0 and ArcGIS 10.1. SfM height (SfMz) was subtracted from ground

203 height (GSz) for 7761 independently surveyed data validation spot heights derived

204 by total station survey (Fig. 3a) providing a vertical difference. The vertical difference

205 was converted into a raster surface with a 2.1 m cell size using an ordinary kriging

206 function in ArcGIS 10.1. This allowed the vertical difference to be visualised. RMSE

207 (root mean square error) and MD (mean difference) were calculated for the vertical

208 difference (SfMz−GSz). Two zones of contrasting vegetation cover (Z1 and Z2; Fig.

209 3a) were mapped from orthorectified aerial imagery, and used to quantify vertical

210 difference associated with contrasting vegetation types. Z1 is characterised by a

211 continuous ground cover of heather, gorse, and occasional shrub and is located on

212 the western side of Llyn Idwal. Z2 consists of grassland and exposed bedrock, and is

213 also located on the western side of Llyn Idwal.

214

4 Results

The dense point cloud was composed of 31,474,859 unique points. With the exception of the extremities of the model, the effective overlap was > 9 images per point. 'Noisy' anomalies are present where the surface of reflective water-bodies are reconstructed. The orthorectified images had a 0.022 m per pixel resolution, and the DSM as seen in Fig. 3b had a 0.088 m per pixel resolution. These resolutions were achieved from an average flight altitude of 117.282 m AGL as reconstructed from the imagery. Discrepancy between the target flight attitude and actual flight attitude is likely to be caused by the use of low resolution Google Earth elevation data for flight planning, and error associated with the use of barometric pressure sensors for determining relative height (see DJI, 2013). Photoscan reported a total RMSE value of 0.033 m, calculated from the 19 SfM GCPs. The total x and y RMSE values reported by Photoscan were 0.019 and 0.020 m respectively. The total vertical RMSE value was 0.018 m.

Spot heights (n = 7761) from the ground survey (GSz) and DSM (SfMz) are in broad agreement, although the vertical difference is a higher than that reported by the 19 SfM GCPs used during the image processing stage. The vertical difference is visualised in Fig. 3c. The dense point cloud provides a vertical RMSE value of 0.517 m (Table 1). The differences for the DSM are offset from zero, with a mean difference of 0.454 m. The majority of the height values on the DSM were within the ± 1 m range (99.8%). However, only 55.4% of the SfM DSM values were within ± 0.5 m of the ground survey data. Isolated spot heights were found to be as much as − 0.705 m under the actual ground survey (GSz) and as much as 4.347 m over.

239 When vertical RMSE is calculated separately, RMSE for the east (less densely
240 vegetated) is significantly lower (RMSE = 0.200; n = 1988), than the west (RMSE =
241 0.588; n = 5773) with 98.8% of height values for the east falling within the ± 0.5 m
242 range (Fig. 4).

243

244 Two contrasting vegetation zones (Z1 and Z2 in Fig. 3a) were investigated. Z1 had
245 an RMSE value of 0.789 m (n = 244). In contrast, Z2 produced a lower RMSE value
246 of 0.362 m (n = 205). The calculated RMSE values for slopes gentler than 20° and
247 those steeper than or equal to 20° were examined for both patches. The values are
248 0.031 and 0.030 m higher for slopes steeper than 20° regardless of the vegetation
249 type. Where RMSE was calculated for separate 10° bins for the entire dataset (7761
250 observations), excluding the 60–70° bin, the reported RMSE value increases on
251 progressively steeper slopes (0.444 to 0.838; Table 2). The 80–90° bin comprised
252 one observation, which shows a high vertical difference (2.222 m).

253

254 An additional analysis of the DSM derived from the sparse point cloud (2,058,037
255 points) was conducted. The sparse point cloud produced a coarser resolution DSM
256 at 0.258 m per pixel. Unlike the dense point cloud, the sparse point cloud did not
257 produce 'noisy' anomalies related to reflective water-bodies. Points from the SfM
258 DSM and the ground survey data were also in broad agreement with 98.9% of the
259 data within the ± 1 m range, and 58.5% of the data in the ± 0.5 m range. The total
260 vertical RMSE value was 0.505 m. The sparse point cloud derived DSM produced a
261 wider range of outlying values, with minimum and maximum anomalies of − 3.416
262 and 3.782 m.

5 Discussion

5.1 Causes of vertical disagreement

Causes of poor surface representation and vertical disagreement between the two data sets have been investigated and include: (1) vegetation; (2) slope angle; and (3) unintentional random error related to the acquisition of the original total station dataset. Vegetation is a known cause of poor surface representation in DEMs derived from both photogrammetry (Lane, 2000; Marzolff and Poesen, 2009), and airborne LiDAR (Lui, 2008; Spaete et al., 2011; Hladik and Alber, 2012). A visual assessment of high vertical difference against the orthorectified imagery shows that error is particularly pronounced around trees, and in areas vegetated with heather (Fig. 5a). Dense vegetation types obstruct line-of-sight of actual ground level, thus generate a vertical difference between the two datasets (Table 1). This difference generated by vegetation is also apparent when the east (sparsely vegetated) and west (densely vegetated) are visualised together (Fig. 3c) or where RMSE is calculated for the two zones of contrasting vegetation (Z1 and Z2). For the examples of Z1 (heather and other shrubs) and Z2 (grasses and exposed bedrock), the presence of a thick covering of vegetation produces an additional 0.434 m RMSE value (Table 1). Whilst the total station data provides information that can be used to produce a bare earth DEM of the moraines, the data presented from SfM photogrammetry accounts for the surface plus vegetation, and therefore represents a DSM. Fig. 5a exemplifies this error, showing how a ground survey point located under a silver birch generates a vertical difference between the two datasets. Similarly, in other areas of the Cwm Idwal DSM, this problem arises due to tilted bedrock rafts with near vertical and in places overhanging sides (Fig. 5b), generating the outlying vertical difference of 4.347 m. As DSMs are essentially 2.5 dimensional

288   representations of the earth's surface and associated surface features, true 3

289   dimensional representation of overhanging surfaces is not possible (Bernhardsen,

290   2002). If the same SfM approach was applied to un-vegetated terrain (e.g. braided

291   channels in Javernick et al., 2014), a significantly lower degree of vertical difference

292   would be expected.

293

294   Further vertical differences between the two topographic datasets is also likely to be

295   the result of unintentional random errors in the ground survey dataset caused by the

296   reflector detail pole not being held perfectly level during point acquisition. The

297   vertical difference caused by this operational error appears to be exacerbated on

298   steep slopes (Table 2). For example, on a perfectly horizontal surface, if the reflector

299   (with the detail pole set to the minimum high of 1.3 m) was inclined at 10° from

300   vertical opposed to being perfectly vertical, the calculated positional and vertical

301   errors would be 0.226 and 0.020 m respectively. However, if the detail pole was

302   inclined at 10° from vertical on a slope of 30°, the expected vertical error would reach

303   the decimetre range. As 16.3% of the 7761 observations were made on slopes >

304   30°, additional errors should be expected. An example where positional

305   misregistration between the two datasets has occurred is presented in Fig. 5c. Here

306   points taken in the vicinity of a steep-sided tilted bedrock raft with near vertical

307   slopes have resulted in vertical disagreement exceeding 1 m. In this circumstance,

308   sub-decimetre positional errors on the ground survey data or poorly resolved

309   features on the SfM DSM promote a high degree of localised vertical disagreement

310   between the two datasets.

311   *5.2 Benefits and practical considerations*

312   The sUAS-SfM technique is in many ways superior to a conventional total station

313   ground survey and performed comparably to a range of recent SfM data validation

314   studies (Table 3). Whilst the total station topographic survey reported by Graham

315   and Midgley (2000) took approximately 15 field-days, this aerial survey was

316   completed in 3 days and also provided high-resolution aerial imagery. The

317   standalone sUAS survey could have feasibly been completed in one day, however

318   this survey needed to be tied into the arbitrary coordinate system and datum used by

319   Graham and Midgley (2000). Operation of the sUAS is unfortunately restricted to dry

320   conditions, with relatively low wind speeds (< 8 ms^{-1}). Despite specific weather

321   requirements, multi-rotor based systems appear to be well-suited to mountain

322   settings. They can be deployed where there is limited space for take-off and landing,

323   and offer a high-degree of control, which is beneficial when surveying in close

324   proximity to steep slopes. Regardless of the sUAS platform used for image

325   acquisition, the technique lends itself to surveying unstable or inaccessible terrain

326   where traditional survey methods would be unfeasible or unsafe.

327

328   UAS based image acquisition has clear benefits over existing full-scale airborne

329   image acquisition as the low survey altitude circumvents much of the weather

330   dependency (particularly cloud coverage) that affect full-scale airborne surveys

331   (Baltsavias, 1999). UAS also have the additional co-benefits of being less costly to

332   deploy in comparison to full scale airborne surveys and have the ability to produce

333   data products that are more scale appropriate for micro topographic investigations

334   than those provided by airborne LiDAR (Laliberte and Rango, 2009; Anderson and

335 Gaston, 2013). However, application of the SfM technique may be limited in some

336 geomorphological environments due to the presence of texturally 'smooth' or

337 reflective surfaces (e.g. snow cover or sand) which prohibit the extraction of

338 meaningful topographic data (Fonstad et al., 2013). Further work to investigate the

339 performance of automated image alignment over more texturally homogenous

340 surfaces may be beneficial where GPS information for camera positions are not

341 available. Care must be taken when acquiring coordinates for the GCPs used during

342 the image processing stage, due to the potential for erroneous readings to propagate

343 through the various derivative data products. Providing that the GCPs are accurately

344 surveyed, the automated nature of the approach is beneficial as it reduces the

345 potential for unintentional random error (e.g. as found to occur in the total station

346 dataset).

347

348 Although the production of a DSM from a dense point cloud produced a sub-

349 decimetre DSM, a coarser DSM (0.258 m per pixel) can be reconstructed from a

350 sparse point cloud of 2 million points with comparable error to that derived from a

351 dense point cloud of 30 million points. Where computational resources for both

352 image processing and data handling are limited or where data are not required at

353 sub decimetre resolution, producing DSMs from lower point densities maybe

354 desirable. The DSM presented here required ~ 7 h to point match and align the 543

355 images. An additional 43 min of processing time was needed to derive the dense

356 point cloud. Research to investigate the influence of point cloud density and the

357 resulting DSM error merits further investigation, although all DSMs should be

358 regarded as an abstraction, with some associated uncertainty (Fisher and Tate,

359 2006; Wechsler, 2007)

5.3 sUAS–SfM as a tool for geomorphological mapping and monitoring

morphometric change

The sUAS–SfM based approach appears to be a useful research tool that aids the production of accurate geomorphological maps. A variety of data sources can be used to compile geomorphological maps (Oguchi et al., 2011), with remotely sensed data often requiring ground-truthing to ensure that landforms are accurately recognised within a study area (Hubbard and Glasser, 2005; Knight et al., 2011). From this perspective the recent availability of high-resolution airborne LiDAR datasets are seen to be beneficial for the production of more accurate geomorphological maps (Jones et al., 2007; Bishop et al., 2012), yet the limited coverage of LiDAR surveys mean researchers do not always have access to high-resolution data. In such cases the sUAS–SfM approach could be utilised by researchers who wish to produce their own ultra-high-resolution DSMs and orthophotos to aid field-mapping campaigns. Researchers should determine whether the spatial coverage offered by sUAS is useful for their investigation. Here, a localised area of 0.211 km^2 was surveyed over four separate flights. This is unlikely to be sufficient for all geoscientific applications, however as sUAS technology improves, greater survey coverage per flight may be permitted.

A further application of sUAS–SfM based surveys is morphometric change detection due to how readily the technique can be deployed for use. Quantification of geomorphological change through the comparison of multi-temporal DEMs is a well-established practice applied to a range of geomorphological settings (coastal, glacial, hillslope, fluvial, etc.; e.g. Pyle et al., 1997; Schiefer and Gilbert, 2007; Dewitte et al.,

384 2008; Marzolff and Poesen, 2009; Mitasova et al., 2009; Hugenholtz, 2010; Irvine-
385 Fynn et al., 2011; Carrivick et al., 2012). In some cases quantifying morphometric
386 change can be problematic where the rate of change is below or close to the
387 achievable accuracy of a given topographic survey technique (Williams, 2012). SfM
388 integrated with sUAS based image acquisition has recently been used for change
389 detection. For example, Whitehead et al. (2013) successfully completed repeat SfM
390 surveys to report on the thinning and motion of Fountain Glacier (Alaska) over a one
391 year period, with the first survey utilising a fixed wing UAS for image acquisition.
392 Lucieer et al. (2013) also used the sUAS–SfM approach, comparing multi-temporal,
393 multi-rotor derived aerial images to monitor landslide displacements at sub-
394 decimetre accuracies. The now widespread availability of aerial platforms and SfM
395 packages adds the range of mapping and survey techniques available to
396 geomorphologists. The technique is a logical choice due to the achievable survey
397 accuracies and potential to monitor geomorphological change at smaller spatial
398 scales remotely.

399

400 **6 Conclusions**

401 The integrated use of sUAS and SfM technologies for the acquisition of sub-
402 decimetre resolution DSMs has been investigated. The technique is shown to be
403 superior to conventional total station survey in terms of resolution, time required for
404 data acquisition, and has the additional benefit of providing ultra-high-resolution
405 orthorectified aerial imagery. DSM spatial resolutions of 0.088 m were achieved from
406 an approximate flight altitude of 117 m AGL whilst using a consumer-grade 18 MP
407 digital camera. Unintentional random error on the total station dataset, vegetation

408 and steep terrain are shown to promote vertical disagreement between the two

409 datasets. Where vegetation is sparse, a vertical difference of 0.200 m RMSE was

410 achieved. Overall, the technique is shown to provide exceptionally high-resolution

411 topographic datasets and aerial imagery. The repeatability of the technique where

412 surveys can be benchmarked or georeferenced using dGPS could offer not only

413 unprecedented spatial resolutions, but also high temporal resolution for monitoring

414 on-going geomorphological processes in a range of environments.

415

References

Anderson, K and Gaston, K.J. 2013. Lightweight unmanned aerial vehicles will revolutionize spatial ecology. *Frontiers in Ecology and the Environment*, **11** (3), 138-146. http://dx.doi.org/10.1890/120150

Aber, J.S., Marzolff, I., Ries, J.B. 2010. Small-format aerial photography: Principles, techniques and geoscience applications. Elsevier, Amsterdam, pp 268.

Addison, K. 1988. The Ice Age in Cwm Idwal, 2nd edition. Shropshire; pp 16.

Agisoft. 2013. Agisoft PhotoScan User Manual: Professional Edition. Retrieved 23/10/2013: http://www.agisoft.ru/products/photoscan/professional/

Baltsavias, E.P. 1999. A comparison between photogrammetry and laser scanning. *ISPRS Journal of Photogrammetry and Remote Sensing*. **54** (2–3), 83-94. http://dx.doi.org/10.1016/S0924-2716(99)00014-3

Bendle, J.M and Glasser, N.F. 2012. Palaeoclimatic reconstruction from Lateglacial (Younger Dryas Chronozone) cirque glaciers in Snowdonia, North Wales. *Proceedings of the Geologists' Association*, **123**, 130-145. http://dx.doi.org/10.1016/j.pgeola.2011.09.006

449 Bernhardsen, T. 2002. *Geographic Information Systems: An Introduction*, John Wiley

450 & Sons: New York, pp 448.

451

452 Bishop, M.P., James, L.A., Shroder Jr, J.F. and Walsh, S.J. 2012. Geospatial

453 technologies and digital geomorphological mapping: Concepts, issues and research.

454 *Geomorphology*. **137**(1), 5-26. http://dx.doi.org/10.1016/j.geomorph.2011.06.027

455

456 CAA. 2012. CAP 722 Unmanned aircraft system operations in UK airspace -

457 guidance (5th Edition). The Stationery Office, Norwich. pp 110.

458

459 Carrivick J.L., Geilhausen, M., Warburton, J., Dickson, N.E., Carver, S.J., Evans,

460 A.J. and Brown, L.E. 2012. Contemporary geomorphological activity throughout the

461 proglacial area of an alpine catchment. *Geomorphology*. **188**, 83-95.

462 http://dx.doi.org/10.1016/j.geomorph.2012.03.029

463

464 Carrivick, J.L., Smith, M.W., Quincey, D.J. and Carver, S.J. 2013. Developments in

465 budget remote sensing for the geosciences. *Geology* Today, **29** (4), 138-143.

466 http://dx.doi.org/10.1111/gto.12015

467

468 Dandois, J.P. and Ellis, E.C. 2013. High spatial resolution three-dimensional

469 mapping of vegetation spectral dynamics using computer vision. *Remote Sensing of*

470 *Environment*. **136**, 259-276. http://dx.doi.org/10.1016/j.rse.2013.04.005

471

472 Darwin, C. 1842. Notes on the effects produced by the ancient glaciers of
473 Caernavonshire, and on boulders transported by floating ice. *Philosophical*
474 *Magazine*, **3**, 180-188.

475

476 Dewitte, O., Jasselette, J.-C., Cornet, Y., Van Den Eeckhaut, M., Collignon, A.,
477 Poesen, J. and Demoulin, A. 2008. Tracking landslide displacements by multi-
478 temporal DTMs: A combined aerial stereophotogrammetric and LIDAR approach in
479 western Belgium. *Engineering Geology*. **99** (1-2), 11-22.

480

481 DJI. 2013. WooKong-M Waypoint-Altitude Offset Setting. Retrieved: 23/02/2014.
482 http://wiki.dji.com/en/index.php/WooKong-M_Waypoint-Altitude_Offset_Setting

483

484 Escritt, E.A. 1971. Plumbing the depths of Idwal's moraines. *Geographical*
485 *Magazine*, **44**, 52-55.

486

487 Fonstad, M.A., Dietrich, J.T., Courville, B.C., Jensen, J.L., Carbonneau, P.E. 2013.
488 Topographic structure from motion: a new development in photogrammetric
489 measurement. *Earth Surface Processes and Landforms*, **38**, 421-430.
490 http://dx.doi.org/10.1002/esp.3366

491

492 Fisher, P.F. and Tate, N.J. 2006. Causes and consequences of error in digital
493 elevation models. *Progress in Physical Geography*. **30** (4), 467-489.
494 http://dx.doi.org/10.1191/0309133306pp492ra

495

496 Graham, D.J. and Midgley, N.G. 2000. Moraine-mound formation by englacial

497 thrusting: the Younger Dryas moraines of Cwm Idwal, North Wales. In: A.J. Maltman,

498 B. Hubbard and M.J. Hambrey (eds.), Deformation of Glacial Materials. London:

499 Geological Society, pp. 321-336. http://dx.doi.org/10.1144/GSL.SP.2000.176.01.24

500

501 Gray, J.M. 1982. The last glaciers (Loch Lomond Advance) in Snowdonia, North

502 Wales. *Geological Journal*, **17**, 111-133. http://dx.doi.org/10.1002/gj.3350170204

503

504 Harwin, S. and Lucieer, A. 2012. Assessing the Accuracy of Georeferenced Point

505 Clouds Produced via Multi-View Stereopsis from Unmanned Aerial Vehicle (UAV)

506 Imagery. *Remote Sensing*, **4**, 1573-1599. http://dx.doi.org/10.3390/rs4061573

507

508 Hladik, C. and Alber, M. 2012. Accuracy assessment and correction of a LIDAR-

509 derived salt marsh digital elevation model. *Remote Sensing of Environment*. **121**,

510 224-235. http://dx.doi.org/10.1016/j.rse.2012.01.018

511

512 Hubbard, B. and Glasser, N. 2005. Field techniques in glaciology and glacial

513 geomorphology. New York, John Wiley & Sons.

514

515 Hugenholtz, C.H. 2010. Topographic changes of a supply-limited inland parabolic

516 sand dune during the incipient phase of stabilization. *Earth Surface Processes and*

517 *Landforms*. **35**, (14), 1674-1681. http://dx.doi.org/10.1002/esp.2053

518

519 Hugenholtz, C.H., Whitehead, K., Brown, O.W., Barchyn, T.E., Moorman, B.J.,

520 LeClair, A., Riddell, K., Hamilton, T. 2013. Geomorphological mapping with a small

521 unmanned aircraft system (sUAS): Feature detection and accuracy assessment of a

522 photogrammetrically-derived digital terrain model, *Geomorphology*, **194**, 16-24.

523 http://dx.doi.org/10.1016/j.geomorph.2013.03.023

524

525 Irvine-Fynn, T.D.L,. Barrand, N.E., Porter, P.R., Hodson, A.J., and Murray, T. 2011.

526 Recent High-Arctic proglacial sediment redistribution: a process perspective using

527 airborne   lidar.   *Geomorphology*,   **125**,   27-39.

528 http://dx.doi.org/10.1016/j.geomorph.2010.08.012

529

530 James, M.R and Robson, S. 2012. Straightforward reconstruction of 3D surfaces and

531 topography with a camera: Accuracy and geoscience application. *Journal of*

532 *geophysical Research*. **117:** F03017. http://dx.doi.org/10.1029/2011JF002289

533

534 Javernick, L., Brasington, J. and Caruso, B. 2014. Modelling the topography of

535 shallow   braided   rivers   using   Structure-from-Motion   photogrammetry.

536 *Geomorphology*.   In   press.   Corrected   Proof.

537 http://dx.doi.org/10.1016/j.geomorph.2014.01.006

538

539   Jones, A.F., Brewer, P.A., Johnstone, E. and Macklin, M.G. 2007. High-resolution

540   interpretative geomorphological mapping of river valley environments using airborne

541   LiDAR data. *Earth Surface Processes and Landforms*. **32** (10): 1574-1592.

542   http://dx.doi.org/10.1002/esp.1505

543

544   Knight, J., Mitchell, W.A. and Rose, J. 2011. Geomorphological field mapping. In:

545   Smith, M.J., Paron, P. and Griffiths, J. (eds) Geomorphological Mapping: a handbook

546   of techniques and applications, Elsevier, London, 151-187.

547

548   Lane, S.N. 2000. The measurement of river channel morphology using digital

549   photogrammetry. *Photogrammetric Record.* **16** (96), 937-961.

550   http://dx.doi.org/10.1111/0031-868X.00159

551

552   Laliberte, A.S. and Rango, A. 2009. Texture and Scale in Object-Based Analysis of

553   Subdecimeter Resolution Unmanned Aerial Vehicle (UAV) Imagery. *IEEE*

554   *Transactions on Geoscience and Remote Sensing*, **47** (3), 761-770.

555   http://dx.doi.org/10.1109/TGRS.2008.2009355

556

557   Leica. 1997. TC600/800 Electronic Total Station User Manual. Lecia Geosystems,

558   Heerbrugg. 135pp.

559

560   Lucieer, A., de Jong, S.M, and Turner, D. 2013. Mapping landslide displacements

561   using Structure from Motion (SfM) and image correlation of multi-temporal UAV

562   photography. *Progress in Physical Geography*. **38** (1), 97-116.

563   http://dx.doi.org/10.1177/0309133313515293

564

565   Lucieer, A., Turner, D., King, D.H. and Robinson, S.A. 2014. Using an Unmanned

566   Aerial Vehicle (UAV) to capture micro-topography of Antarctic moss beds.

567   *International Journal of Applied Earth Observation and Geoinformation*, **27A**, 53-62.

568   http://dx.doi.org/10.1016/j.jag.2013.05.011

569

570   Lui, X. 2008. Airborne LiDAR for DEM generation: some critical issues. *Progress in*

571   *Physical Geography*. **32** (1), 31-49. http://dx.doi.org/10.1177/0309133308089496

572

573   Mancini. F., Dubbini, M., Gattelli, M., Stecchi, F., Fabbri, S. and Gabbianelli, G.

574   2013. Using Unmanned Aerial Vehicles (UAV) for High-Resolution Reconstruction of

575   Topography: The Structure from Motion Approach on Coastal Environments. *Remote*

576   *Sensing*, **5**, 6880-6898. http://dx.doi.org/10.3390/rs5126880

577

578   Marzolff, I. and Poesen, J. 2009. The potential of 3D gully monitoring with GIS using

579   high-resolution aerial photography and a digital photogrammetry system.

580   *Geomorphology*, **111** (1-2), 48-60. http://dx.doi.org/10.1016/j.geomorph.2008.05.047

581

582 Mitasova, H., Overton, M.F., Recalde, J.J., Bernstein, D.J and Freeman, C.W. 2009.

583 Raster-Based Analysis of Coastal Terrain Dynamics from Multitemporal Lidar Data.

584 *Journal of Coastal Research*. **25** (2), 507-514. http://dx.doi.org/10.2112/07-0976.1

585

586 Niethammer, U., James, M.R., Rothmund, S., Travelletti, J. and Joswig, M. 2012.

587 UAV-based remote sensing of the Super-Sauze landslide: Evaluation and results.

588 *Engineering Geology*, **128**, 2-11. http://dx.doi.org/10.1016/j.enggeo.2011.03.012

589

590 Oguchi, T., Hayakawa, Y.S. and Wasklewicz, T. 2011. Data Sources. In: Smith, M.J.,

591 Paron, P. and Griffiths, J. (eds) Geomorphological Mapping: a handbook of

592 techniques and applications, Elsevier, London, 151-187.

593

594 Ouédraogo, M.M., Degré, A., Debouche, C. and Lisein, J. 2014. The evaluation of

595 unmanned aerial system-based photogrammetry and terrestrial laser scanning to

596 generate DEMs of agricultural watersheds. *Geomorphology*, **214**, 339–355.

597 http://dx.doi.org/10.1016/j.geomorph.2014.02.016

598

599 Pyle, C.J., Richards, K.S. and Chandler, J.H. 1997. Digital photogrammetric

600 monitoring of river bank erosion. *The Photogrammetric Record*. **15**, 753–764.

601 http://dx.doi.org/10.1111/0031-868X.00083

602

603   Rango, A., Laliberte, A., Herrick, J.E., Winters, C., Havstad, K., Steele, C. and

604   Browning, D. 2009. Unmanned aerial vehicle-based remote sensing for rangeland

605   assessment, monitoring and management. *Journal of Applied Remote Sensing*: **3**, 1-

606   15. http://dx.doi.org/10.1117/1.3216822

607

608   Rosnell, T and Honkavaara, E. 2012. Point Cloud Generation from Aerial Image

609   Data Acquired by a Quadrocopter Type Micro Unmanned Aerial Vehicle and Digital

610   Still Camera. *Sensors*, **12**, 453-480. http://dx.doi.org/10.3390/s120100453

611

612   Rhind, P. and Jones, B. The vegetation history of Snowdonia since the Last Glacial

613   Period. *Field Studies*, **10**, 539-552.

614

615   Schiefer, E. and Gilbert, R. 2007. Reconstructing morphometric change in a

616   proglacial landscape using historical aerial photography and automated DEM

617   generation. **88** (1-2), 167-178. http://dx.doi.org/10.1016/j.geomorph.2006.11.003

618

619   Smith, M.J., Chandler, J. and Rose, J. 2009. High spatial resolution data acquisition

620   for the geosciences: kite aerial photography. *Earth Surface Processes and*

621   *Landforms*. **34**, 155-161. http://dx.doi.org/10.1002/esp.1702

622

623 Snavely, N., Seitz, S.M. and Szeliski, R. 2008. Modelling the World from Internet

624 Photo Collections. *International Journal of Computer Vision*. **80** (2), 189-210.

625 http://dx.doi.org/10.1007/s11263-007-0107-3

626

627 Spaete, L.P., Glenn, N.F., Derryberry, D.R., Sankey, T.T., Mitchell, J.J., and

628 Hardegree, S.P. 2011. Vegetation and slope effects on accuracy of a LiDAR-derived

629 DEM in the sagebrush steppe. *Remote Sensing Letters*, **2** (4), 317-326.

630 http://dx.doi.org/10.1080/01431161.2010.515267

631

632 Tarolli, P. 2014. High-resolution topography for understanding Earth surface

633 processes: opportunities and challenges. *Geomorphology*, **216**, 295-312.

634 http://dx.doi.org/10.1016/j.geomorph.2014.03.008

635

636 Turner, D., Lucieer, A. and Watson, C. 2012. An Automated Technique for

637 Generating Georectified Mosaics from Ultra-High Resolution Unmanned Aerial

638 Vehicle (UAV) Imagery, Based on Structure from Motion (SfM) Point Clouds. *Remote*

639 *Sensing*, **4**, 1392-1410. http://dx.doi.org/10.3390/rs4051392

640

641 Wechsler, S.P. 2007. Uncertainties associated with digital elevation models for

642 hydrologic applications: a review. *Hydrology and Earth System Sciences*, **11**, 1481-

643 1500. http://dx.doi.org/10.5194/hess-11-1481-2007

644

645 Westoby, M.J., Brasington, J., Glasser, N.F., Hambrey, M.J., and Reynolds, J.M.
646 2012. 'Structure-from-motion' photogrammetry: A low-cost, effective tool for
647 geoscience applications. *Geomorphology*: **179**, 300-314.
648 http://dx.doi.org/10.1016/j.geomorph.2012.08.021

649

650 Wester-Ebbinghaus, W. 1980. Aerial Photography by radio controlled model
651 helicopter. London. England. *The Photogrammetric Record*. Vol. X No. 55.
652 http://dx.doi.org/10.1111/j.1477-9730.1980.tb00006.x

653

654 Whitehead, K., Moorman, B.J. and Hugenholtz, C.H. 2013. Brief Communication:
655 Low-cost, on-demand aerial photogrammetry for glaciological measurement. *The*
656 *Cryosphere*, **7**, 1879-1884. http://dx.doi.org/10.5194/tc-7-1879-2013

657

658 Williams, R.D. 2012. Section 2.3.2: DEMs of difference (using DODs to quantify
659 landscape change and uncertainty analysis in DoDs). In: Clarke, L.E & Nield, J.M.
660 (Eds.) Geomorphological Techniques (Online Edition). British Society for
661 Geomorphology; London, UK. ISSN: 2047-0371.

662   **Fig. 1** Maps showing the study site location in relation to (a) North-west Europe, and

663   (b) North Wales. ©Crown Copyright/database right 2014. An Ordnance

664   Survey/EDINA supplied service. (c) A ground-level panoramic photograph of the

665   moraine-mound complex which is located on both the left and right of Llyn Idwal.

666

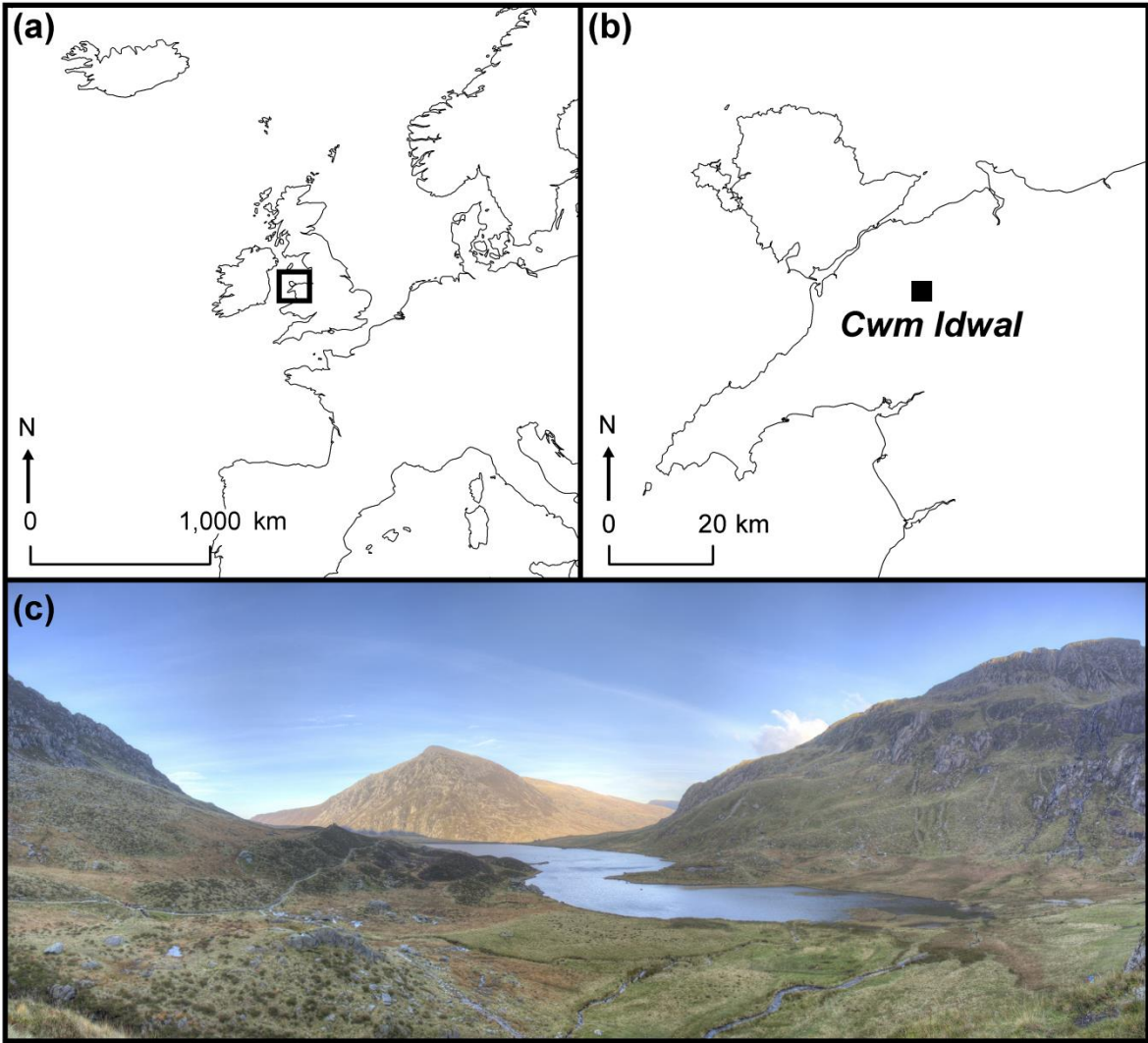667   **Fig. 2** A schematic drawing of the S800 hexacopter.

668

669   **Fig. 3** Maps displaying the topographic data and analysis of vertical disagreement.

670   (a) The distribution of 7761 ground-survey points and 19 SfM ground-control points

671   across the survey area. Two zones (Z1 and Z2) of distinct ground cover are

672   delimited. (b) A hillshaded DSM at 0.088 m per pixel resolution derived from the

673   sUAS–SfM survey. (c) A raster surface of vertical difference produced using an

674   ordinary kriging function at a resolution of 2.1 m per pixel. The spatial extent of the

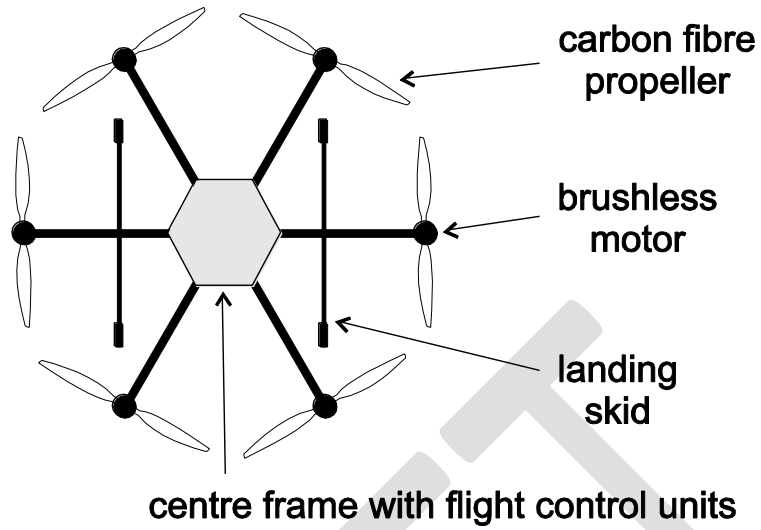675   spot heights is delimited by the dashed line.

676

677   **Fig. 4** The occurrence of vertical difference in association with: (a) vegetation, (b)

678   near vertical and in places partially overhanging bedrock rafts, and (c) positional
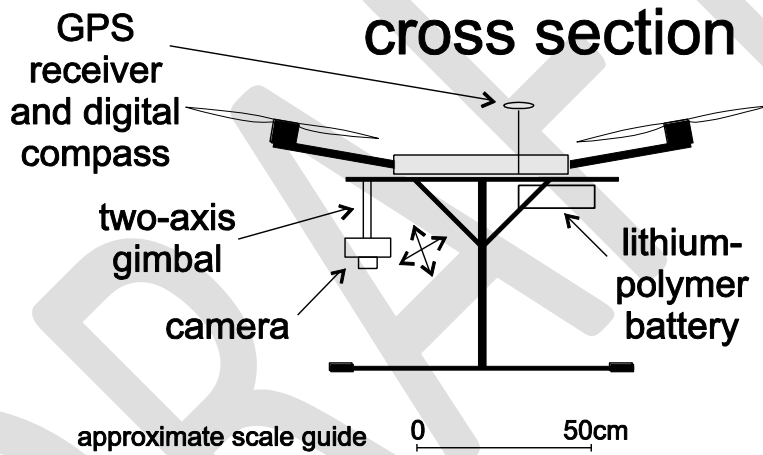
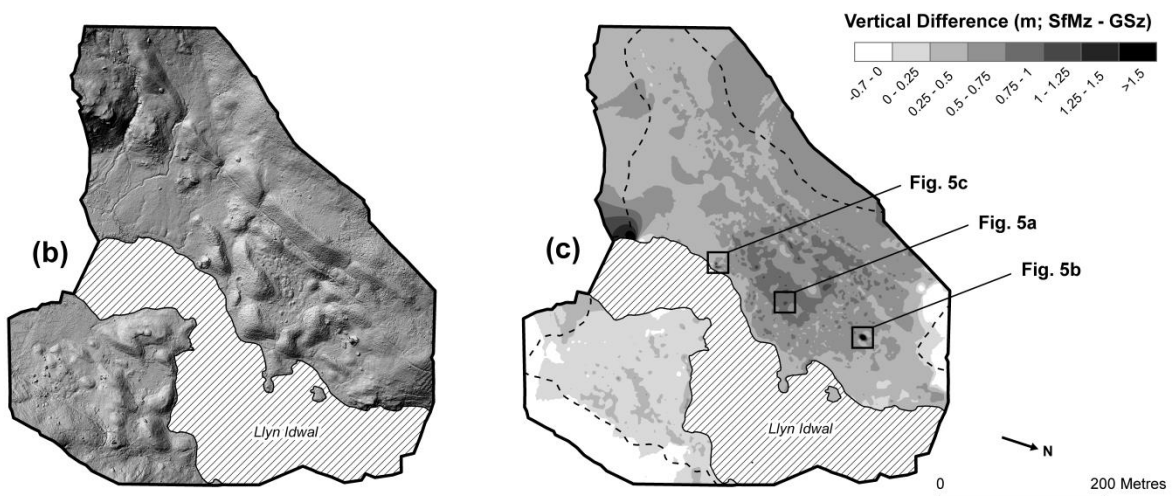679   misregistration close to near vertical slopes

680

681

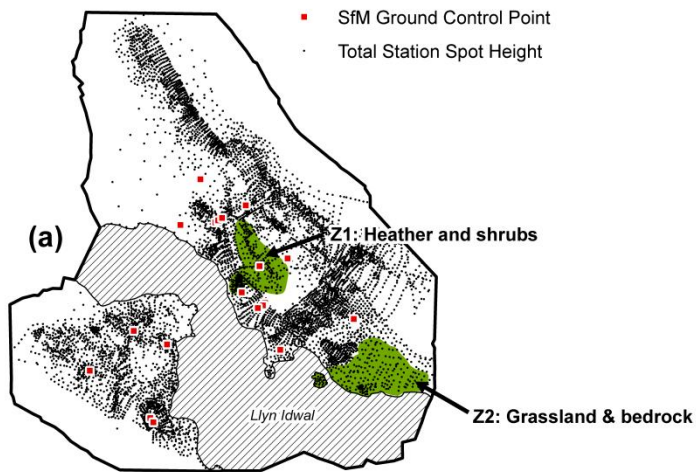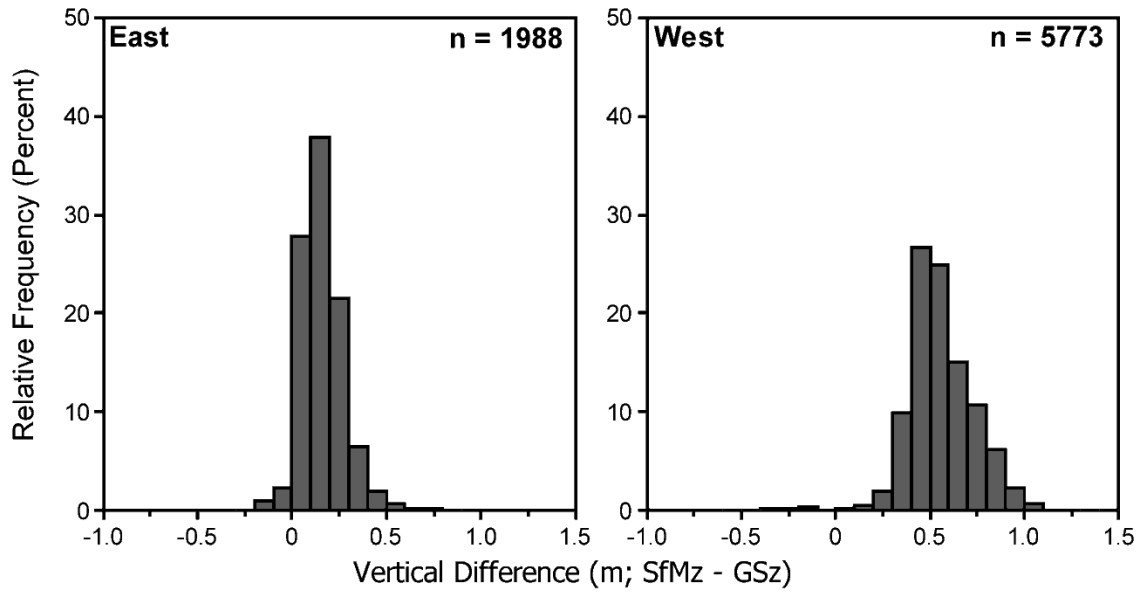## plan view

carbon fibre
propeller

brushless
motor

landing
skid

centre frame with flight control units

cross section

GPS
receiver
and digital
compass

two-axis
gimbal

camera

lithium-
polymer
battery

approximate scale guide

0   50cm

SfM Ground Control Point
Total Station Spot Height

(a)

Z1: Heather and shrubs

Z2: Grassland & bedrock

Llyn Idwal

(b)

Llyn Idwal

(c)

Llyn Idwal

Vertical Difference (m; SfMz - GSz)

-0.7 - 0   0 - 0.25   0.25 - 0.5   0.5 - 0.75   0.75 - 1   1 - 1.25   1.25 - 1.5   >1.5

Fig. 5c

Fig. 5a

Fig. 5b

N

0   200 Metres

683

684

Vertical Difference (m; SfMz - GSz)

| -0.7 - 0 | 0 - 0.25 | 0.25 - 0.5 | 0.5 - 0.75 | 0.75 - 1 | 1 - 1.25 | 1.25 - 1.5 | >1.5 |

0   10 Metres

● Ground Survey Point

685

686 **Table 1** Statistics for the vertical difference between the Cwm Idwal topographic

687 datasets

Area	Total Observations (n)	RMSE	MD [a]	RMSE (<20º)	RMSE (≥20º)
All	7761	0.517	0.454	0.468 (n = 4527)	0.578 (n = 3234)
East	1988	0.200	0.155	0.169 (n = 1306)	0.247 (n = 682)
West	5773	0.588	0.557	0.544 (n = 3222)	0.639 (n = 2551)
Z1	244	0.796	0.820	0.789 (n = 102)	0.821 (n = 142)
Z2	205	0.362	0.341	0.354 (n = 152)	0.384 (n = 53)

688 [a] *Mean Difference*

689 **Table 2** Calculated RMSE for vertical difference binned by slope angle.

Bin	RMSE	Observations (n)
0 – 9	0.444	1864
10 – 19	0.482	2662
20 – 29	0.543	1967
30 – 39	0.603	952
40 – 49	0.678	263
50 – 59	0.739	36
60 – 69	0.729	10
70 – 79	0.838	6
80 – 90	2.222	1

690

691 **Table 3** Comparative table of known vertical differences between SfM topographic

692 surveys and various validation datasets in a range of geomorphological

693 environments

Study	*Geomorphological setting*	*Camera*	*Camera Platform*	*Survey Altitude (m AGL)*	*Validation Data*	*Vertical Difference*
Westoby et al. (2012)	Coastal	SLR: Model not specified	None	Ground-level	Terrestrial Laser Scanner	94% points values within +/- 1 m
Hugenholtz et al.. (2013)	Aeolian	Olympus PEN Mini E-PM1	Fixed-wing sUAS	200	RTK GPS	RMSE = 0.29 m
Fonstad et al. (2013)	Exposed Bedrock/Fluvial	Canon A480	Helikite	10-70	LiDAR	RMSE = 1.05 m
Javernick et al.. (2014)	Fluvial (Braided Channel)	Canon (10.1 MP): Model not specified.	Full-scale helicopter	600-800	RTK GPS	RMSE = 0.13 – 0.37 m
This study	Glacial landforms (Vegetated)	Canon EOS-M (18 MP)	Multi-rotor sUAS	117 (average)	Total Station	RMSE = East: 0.200 m West: 0.588 m All: 0.517 m

694